

Article

Multi-Proxy Characterisation of the Storegga Tsunami and Its Impact on the Early Holocene Landscapes of the Southern North Sea

Vincent Gaffney ¹, Simon Fitch ¹, Martin Bates ², Roselyn L. Ware ³, Tim Kinnaird ⁴, Benjamin Gearey ⁵, Tom Hill ⁶, Richard Telford ¹, Cathy Batt ¹, Ben Stern ¹, John Whittaker ⁶, Sarah Davies ⁷, Mohammed Ben Sharada ¹, Rosie Everett ³, Rebecca Cribdon ³, Logan Kistler ⁸, Sam Harris ¹, Kevin Kearney ⁵, James Walker ¹, Merle Muru ^{1,9}, Derek Hamilton ¹⁰, Matthew Law ¹¹, Alex Finlay ¹², Richard Bates ^{4,*} and Robin G. Allaby ³

- ¹ School of Archaeological and Forensic Sciences, University of Bradford, Bradford BD7 1DP, UK; v.gaffney@bradford.ac.uk (V.G.); s.fitch@bradford.ac.uk (S.F.); r.telford@bradford.ac.uk (R.T.); c.m.batt@bradford.ac.uk (C.B.); B.Stern@bradford.ac.uk (B.S.); M.A.M.BenSharada@bradford.ac.uk (M.B.S.); S.Harris11@student.bradford.ac.uk (S.H.); j.walker17@bradford.ac.uk (J.W.); m.muru@bradford.ac.uk (M.M.)
- ² Faculty of Humanities and Performing Arts, University of Wales Trinity Saint David, Lampeter, Ceredigion, Wales SA48 7ED, UK; m.bates@uwtsd.ac.uk
- ³ School of Life Sciences, Gibbet Hill Campus, University of Warwick, Coventry CV4 7AL, UK; R.Ware.1@warwick.ac.uk (R.L.W.); r.everett@warwick.ac.uk (R.E.); r.cribdon@warwick.ac.uk (R.C.); r.g.allaby@warwick.ac.uk (R.G.A.)
- ⁴ School of Earth and Environmental Sciences, University of St Andrews, St Andrews KY16 9AL, UK; tk17@st-andrews.ac.uk
- ⁵ Department of Archaeology, University College Cork, T12 CY82 Cork, Ireland; b.gearey@ucc.ie (B.G.); kevin. Kearney@umail.ucc.ie (K.K.)
- ⁶ Department of Earth Sciences, Natural History Museum, London SW7 5BD, UK; Thomas.Hill@nhm.ac.uk (T.H.); j.whittaker@nhm.ac.uk (J.W.)
- ⁷ Geography and Earth Sciences, Aberystwyth University, Aberystwyth SY23 3FL, UK; sjd@aber.ac.uk
- ⁸ Department of Anthropology, National Museum of Natural History, Smithsonian Institution, Washington, DC 20560, USA; kistlerl@si.edu
- ⁹ Department of Geography, Institute of Ecology and Earth Sciences, University of Tartu, 51003 Tartu, Estonia
- ¹⁰ SUERC Radiocarbon Dating Laboratory, Scottish Enterprise Park, East Kilbride G75 0QF, UK; derek.hamilton.2@glasgow.ac.uk
- ¹¹ School of Sciences, Bath Spa University, Bath BA2 9BN, UK; m.law@bathspa.ac.uk
- ¹² Chemostrat Ltd., 1 Ravenscroft Court, Buttington Cross Enterprise Park, Welshpool, Powys SY21 8SL, UK; alexfinlay@chemostrat.com
- * Correspondence: crb@st-andrews.ac.uk

Received: 12 June 2020; Accepted: 11 July 2020; Published: 15 July 2020



Abstract: Doggerland was a landmass occupying an area currently covered by the North Sea until marine inundation took place during the mid-Holocene, ultimately separating the British landmass from the rest of Europe. The Storegga Event, which triggered a tsunami reflected in sediment deposits in the northern North Sea, northeast coastlines of the British Isles and across the North Atlantic, was a major event during this transgressive phase. The spatial extent of the Storegga tsunami however remains unconfirmed as, to date, no direct evidence for the event has been recovered from the southern North Sea. We present evidence of a tsunami deposit in the southern North Sea at the head of a palaeo-river system that has been identified using seismic survey. The evidence, based on lithostratigraphy, geochemical signatures, macro and microfossils and sedimentary ancient DNA (sedaDNA), supported by optical stimulated luminescence (OSL) and radiocarbon dating, suggests that these deposits were a result of the tsunami. Seismic identification of this stratum and analysis of adjacent cores showed diminished traces of the tsunami which was largely removed by subsequent

erosional processes. Our results confirm previous modelling of the impact of the tsunami within this area of the southern North Sea, and also indicate that these effects were temporary, localized, and mitigated by the dense woodland and topography of the area. We conclude that clear physical remnants of the wave in these areas are likely to be restricted to now buried, palaeo-inland basins and incised river valley systems.

Keywords: seismic; tsunami; Doggerland; palaeoenvironment; palaeolandscape; sedimentary ancient DNA; geochemistry; geomorphology; Mesolithic; Storegga; North Sea

1. Introduction

The Holocene pre-inundation landscape of the southern North Sea, known as Doggerland, was a gently undulating, low-relief area associated with Mesolithic hunter-gatherer communities [1]. Sea-level rise during the mid-Holocene period at the regional scale was episodic due to local variations in isostatic rebound, autocompaction of sediments and palaeotidal range. The precise timing and extent of such processes and consequently their impact on Mesolithic communities, remains unclear [2]. Toward the end of Doggerland, when the majority of the landscape had already been lost, the remaining land would have been low lying, close to sea level, extending out from Norfolk, UK, to an archipelago centred on the Dogger Bank. This low-lying landscape would have therefore been extremely vulnerable to catastrophic flooding events. Significantly, a key regional event during this period was a series of underwater landslides known as the Storegga Event, which occurred off the Norwegian Atlantic coast 8.15 thousand years before present (ka cal BP) [2–5]. This event triggered a tsunami that some researchers have associated with the final submersion of Doggerland [6].

Despite the magnitude of the Storegga tsunami in the northern North Sea, as evidenced by sediment deposits and predicted by model simulations [4,6,7], there has been a surprising lack of physical evidence to suggest the tsunami reached the southern North Sea (Figure 1) [3,8]. Furthermore, whilst the same model suggests that if the tsunami did reach the southern North Sea the actual impact within this area has been the subject of debate [8].

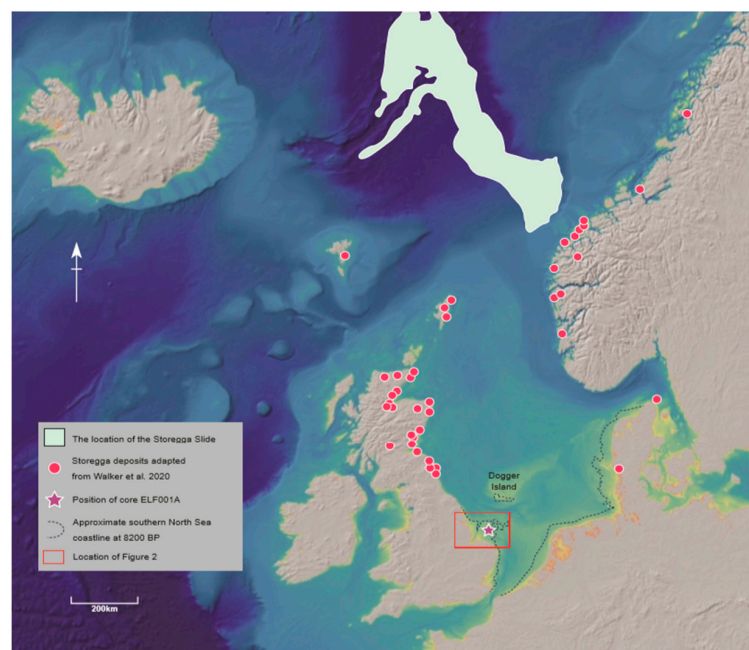


Figure 1. The North Sea, Storegga underwater landslide event run-out, associated deposit locations and core ELF001A. Location of deposits associated with Storegga slip follow data in summarized [8].

The impact of the Storegga tsunami on contemporary landscapes and, by implication, on human communities is clearly of some importance. The recovery of a series of cores within the southern North Sea region, as part of an ERC-funded project Europe's Lost Frontiers, provided an opportunity to assess the significance of the event on the contemporary landscape and, by extension, hunter-gather populations from within what remained of Doggerland.

2. Characterising Tsunami Deposits

Recognition of ancient tsunami deposits presents a considerable challenge in the field. Many of the key sedimentary features that are associated with tsunamis have similarities to those left by other depositional events, for example storm surges [9]. Nonetheless, over the past 20 years several studies of both ancient and modern sediments have identified important discriminators between these events. For example, Fujiwara and Kamataki [10] outlined a tsunami depositional model based on multiple sedimentary features identified in deposits in Tomoe Bay, Japan. Here the salient features of this event were interpreted as resulting from the difference in wave type. Tsunami sequences typically result from a few high-velocity, long-period, and often large amplitude waves where flow depths are greater than 10 m. These events entrained sediment from multiple offshore, shoreface, beach, and landward erosion zones. This often contrasts with storm surges where wave amplitudes are commonly less than 3 m, and sediment is transported primarily as bed-load by traction, from nearshore, shoreface and beach deposits. The resulting textural composition of deposits has been used to distinguish the cause of sedimentation however, the exact coastal morphology, the bathymetry of run up and the availability of sediment can make this challenging.

A common difference between tsunami and storm surges, and upon which most investigators do agree on, is the bi-direction of flow that reflects the multiple land and seaward movement of wave events in a tsunami [9]. In these cases, deposition results from a few high-velocity, long-period waves that deposit successive layers of coarse-grain size. These are separated by deposits fining upwards to mud drapes and each sub-event ends with flow velocity stagnation. In a number of cases at least two main pulses, that are manifest by four graded layers within the overall sequence, have been reported. In contrast, storm deposits typically demonstrate a unidirectional current in a single graded sequence. This generally reflects a gradual and prolonged event consisting of many waves that erode beaches and dunes with no significant overland return flow until after the main flooding. Nanayama et al. [11] illustrate this difference in the study of the 1993 Japan Sea tsunami and the 1959 Miyakojima typhoon. Kortekaas and Dawson [12] record similar sequences related to the Lisbon 1755AD earthquake and subsequent tsunami with overlying storm deposits. Fujiwara and Kamataki [10] also noted vertical stacking of internal structures within Holocene deposits in the Boso Peninsula, Japan. Another common feature of tsunami deposits is the presence of mud rip-up clasts. Goff et al. [13] noted these at a site in New Zealand and Morton et al. [14] advocate their significance from a study of modern tsunami deposits. They also note, in contrast to storm deposits, that a tsunami may show a conformity to the antecedent landscape and a lateral alignment of ripped-up material within the deposit. Investigation of such deposits can be problematic. On land this would involve the recovery of material from multiple sites across significant areas of landscape. Such a methodology is generally not practical in the marine context where access to sites is limited usually due to prohibitive costs of coring. Comparison with local onshore material and coastal storm deposits is recommended, but with inundated palaeolandscapes these 'onshore' areas have often been eroded. A recent study that has addressed this issue by examining a series of offshore cores has recently been presented by Riou et al. [15]. Here the backwash (offshore) sediments resulting from two historic tsunami events was analysed using geochemical and mineralogical analysis, and careful examination of the sediment texture. In most cores, basal soft sediment micro deformation that included asymmetric flame structures were recognised as a key character of the tsunami event.

In distinguishing tsunami-derived deposits we are assisted by Peters and Jaffe's [16] useful database of studies on sedimentary characteristics of recent tsunami deposits. They conclude that while

there are differences between tsunami and storm surges, knowledge of site-specific morphological criteria is also important for discrimination. Physical criteria that may be diagnostic include; deposit thickness and geometry, sediment grain sizes, sorting (grading) and type, sedimentary structures (between bed and within bed), layering (type and organisation of stratification), contacts (both below and above), and composition (macro and micro fossils). Therefore, a multi-proxy study is needed to assure the origin of any sediments as tsunami deposits. A summary of characteristics for distinguishing tsunami and storm deposits is given in Table 1.

Table 1. Typical characteristics for distinguishing tsunami and storm deposits, after Kortekaas and Dawson [12], Morton et al. [14], and Peters and Jaffe [16]. Note, all authors recognise that all features are not observed in each type of event or are necessarily preserved for each event.

| | Tsunami | Storm Surge |
|--------------------------|--|--|
| Physical | | |
| Near shore wave height | 10–20 m, | <10 m |
| Wave period | 100–2000 s | 10–25 s |
| Deepwater wave height | <0.5 m | >5 m |
| Wave run-up height | 10 s m | <5 m |
| Inundation depth | 0–20 m | <5 m |
| Active flow duration | min to h | h-days |
| Overland flood velocity | up to 20 ms ^{−1} | up to 5 ms ^{−1} |
| Length of coast impacted | 10–10,000 km | 100–1000 km |
| Morphology | | |
| Features | Wash-over fans behind breached barriers | Wash-over fans behind breached barriers |
| Stratigraphy | | |
| Lateral continuity | Thins inland and becomes discontinuous | Thins inland |
| Lateral continuity | Fines inland | Fines inland |
| Extent | Large inland extent | Relative smaller inland extent |
| Event thickness | <50 cm | 50–150 cm |
| Geometry | Drapes antecedent topography | Wedges out inland |
| Sedimentology | | |
| Grain size | mud to boulders | sand common but some boulder deposition reported |
| Grading | Typically two or more fining upward sequences, sometimes homogeneous | Typically a single fining upward or homogeneous sequence |
| Mud cap | Mud cap at surface | No mud cap |
| Imbrication | Bi-directional | Unidirectional |
| Sorting | Intraclasts from underlying material | Not found |
| Sorting | Poorly sorted (particle size ranging from mud to boulders); rip up clasts common | Relatively better sorted |
| Transport | Sediment transport mostly suspension, with initial phased dominated by traction and bedload movement | Sediment transport mostly traction throughout, some suspension |
| Structures | Rip-up clasts common | Rip—up clasts absent |
| Base structures | Multi-layer asymmetric flame structures | Single layer flame structures |
| Base structures | Loading structures at base | Not found |
| Base contact | Abrupt basal contact | Abrupt basal contact |
| Structures | Internal sedimentary structures very seldom found | Internal sedimentary structures more common |
| Geochemistry | | |
| Signatures | Increase in geochemical elements indicating marine origin | Increase in geochemical elements indicating marine origin |
| Signature | Si high at base, clay high on final drape | Mixed Si to clay throughout |
| Heavy-mineral deposits | Site specific | Site specific |
| Palaeontology | | |
| Fossils | Marine shell rich units | Marine shell fragments |
| Flora | Terrestrial plant fragments, particularly at base | Plant fragments throughout |
| Flora | Rafting light material | Not found |
| Diversity | Increased diversity (mixture marine and brackish fossils) | Mixture of marine and fresh-water fossils |
| Preservation | Relative well/poorly preserved fossils | Poorly preserved fossils |

The available data can be used to reconstruct a likely scenario to assist in identifying a tsunami deposit. A tsunami event, where the source of water movement is remote to the impact area, shows a typical arrival onshore that begins with a rapid fall in relative sea level causing erosion of near shore material. This is followed by the first wave pulse which brings a mixture of locally derived marine sediment. These include mixed and broken fauna and flora, and particularly shell material. As the wave reaches maximum onshore limits the energy reduces to zero, and this is represented as a fining upwards grading of the bed [17]. The wave then retreats carrying with it an increased terrestrial signature mixed with some of the marine material brought inland by the first wave pulse. The resulting deposit is also marked by a fining upwards sequence as the wave reduces to zero velocity offshore. Subsequent waves repeat the cycle [11], with the second wave often of greater magnitude than the first. Tsunami deposits are therefore typically a repeated sequence of events, but because of the relatively short time window for each cycle, the resulting deposits are rarely greater than 1m thick. This is in contrast to a storm surge which typically only shows one fining-upwards sequence but which can reach over 1m in thickness.

3. Materials and Methods

In order to reconstruct the early Holocene palaeolandscape of the southern North Sea we used a mega-seismic survey (see Supplementary Information, text S1) to identify the coastline at approximately 8.2 ka cal BP and interpolated the results using bathymetric contours from EMODnet [18] and sea level curve data from Bradley et al. [19].

To characterize the landscape inferred from the palaeobathymetric reconstruction, we investigated the seismic signal further by the collection of 15 vibrocores across the landscape. The exact core locations were chosen to allow correlation of the seismic at different palaeogeographic settings and to track the Holocene inundation process. The core most strongly associated with the seismic signal, ELF001A was analysed with the following techniques; grain size measurement using standard dry sieving, loss on ignition, palaeomagnetic (remnant magnetization using a DC 755 superconducting rock magnetometer, 2G Enterprises, Sand City, CA, USA), geochemical scanning (using an XRF core scanner, Itrax, Mölndal, Sweden), organic chemistry profiling for lipid analysis (using a 7890A gas chromatograph, Agilent, Santa Clara, CA, USA, coupled with a 5975C Inert XL mass selective detector), optically stimulated luminescence (OSL) profiling and dating, radiocarbon (RC) dating, foraminifera and ostracod assessment, pollen analysis, diatom analysis, mollusca analysis and sedimentary ancient DNA (sedaDNA) analysis. All methods are described in full detail in the supplementary information texts

4. Results

4.1. Reconstruction of the South-Eastern Doggerland Archipelago

From the mega-seismic survey, bathymetric and sea level data we inferred the landscape illustrated in Figure 2.

The data confirmed that the offshore area associated with Doggerland was, by approximately 8.2 ka cal BP, represented by an archipelago and small stretches of coastal plain off the eastern coast of England. Within the residual plain were a series of palaeochannels representing river systems within glacial valleys that have been incised through Late Devensian terminal moraines [20]. These included a channel associated with the Outer Dowsing Deep, for which we used the term the Southern River. This channel runs north to south terminating in north and south-facing headlands that delineate a central basin with associated low-lying watershed. A restricted area around the central basin was associated with a distinct but discontinuous seismic signal suggestive of an anomalously distinct and partially eroded stratum.

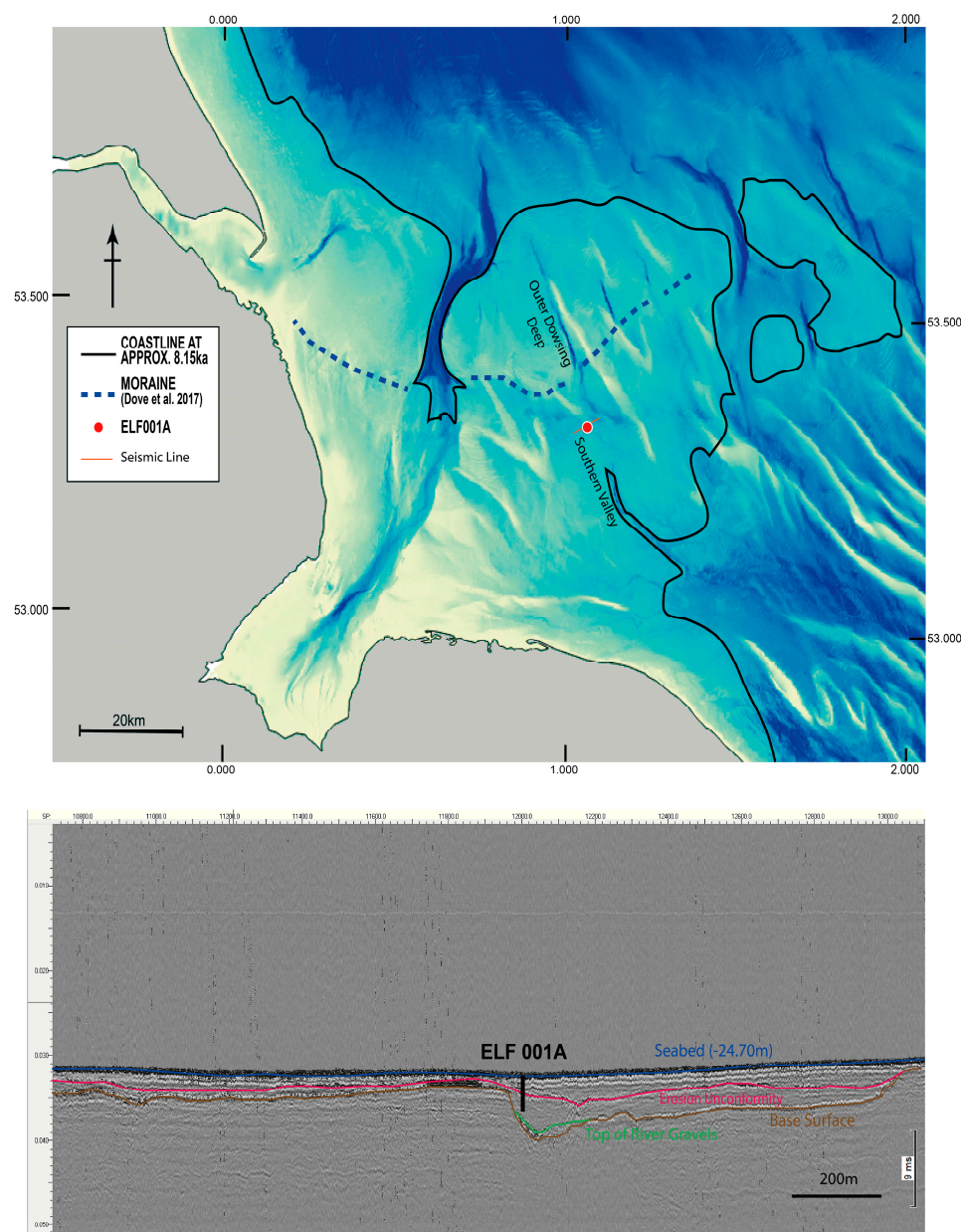


Figure 2. Geomorphological reconstruction of the palaeolandscape off the east coast of England c. 8.2 ka cal BP. Above: Present coast of East England (grey) with offshore area showing the coastline reconstruction at approximately 8.2 ka cal BP, position of moraine ridge (after Dove et al. [20]), location of core and seismic line example. Below: 2D seismic line acquired through core location showing major reflection horizons, base surface and the major erosional boundary identified as a regional event.

4.2. Description of the Core ELF001A

Whilst a full core description is given in Supplementary Information Table S1, a summary is provided here. The base of the core consists of dark grey finely laminated silts and fine sands from 3.5 m to approximately 1.52 m depth beneath seafloor (unit 1a-7). The sub-horizontal laminations, up to 1 cm thick are demarcated by occasional brown organic laminae. At 1.52 m there is a very sharp contact boundary suggestive of an erosional event. Above this contact grey, medium grain sand with freshly broken shell fragments, whole shells and small stones (up to 3 cm in size) exhibit six discrete sequences each of upward-fining sediment (unit 1a-6). At 1.19 m this sequence fines to a dark grey silty sand that is moderately compact (unit 1a-5). At 1.09 m another sharp contact is encountered after

which dark grey very well laminated silty sands once again show horizontal laminations of 2–4 mm thickness (unit 1a-4). From 0.90 m to the surface grey to yellow medium sand is loosely consolidated and shows evidence of bioturbation (units 1a-3 to 1a-1).

4.3. Physical Properties of Core ELF001A

Sediment properties, geochemistry, remnant magnetism and OSL dating results are shown in Figure 3 for the whole core ELF001A and in Figure 4 for the key section of core between depths of 1.00 m and 1.60 m. The geochemical data was acquired at 500 μm resolution but is plotted using a running average of ± 5 mm. A suite of 14 elements had detection limits above background levels including Si, Cl, K, Ca, Ti, Mn, Fe, Ni, Zn, Br, Rb, Sr and Zr. In order to compensate for potential effects of tube aging and beam intensity, the Compton scattering data was ratioed to the Rayleigh scattering data as detailed by Fortin et al. [21] to provide a semi-quantitative density value, ρ , for the sediment. Principal component analysis was conducted (SI Text S2.3) to establish potential environmental indicators inferred from the chemical elements and elemental ratios (SI Text S2.1). Elements showing grouping with discriminative signals included detrital (Si, Ni and Zr), clay (K and Rb), carbonate (Ca and Sr) and oxides (Mn, Fe, Ti and Zn) with elements plotting separately including Br, Cl and S. Sr, Rb, Si and Zr were used to chemically zone the core into key chemo-stratigraphic sequences (Figure 3C).

From a review of geochemical application in tsunami deposit analysis Chagué-Goff et al. [22] suggested that three key ratios of elemental proxies are important, namely:

- Sr/Rb—marine signature reflecting the chemical proxy for aragonite as shell content vs. clay content
- Si/Rb—grain size proxy reflecting the chemical proxy for quartz (coarser sand grain) vs. clay content
- Zr/Sr—a terrestrial vs. marine sediment chemical proxy based on the input of detrital zircons

The ratios were used to chemically zone the core into key chemo-stratigraphic sequences (Figure 4). The base of the core (chemo-stratigraphic zones C6 and C7) contain low Sr, Si and Zr and high Rb abundances indicating that they are composed of fine clay/silt deposits with only occasional shell fragments as a result of relatively low energy marine conditions. There is a sudden chemical change at 1.52 m, spanning 2 cm of section representing an erosional contact after which low energy conditions are abruptly terminated. This is followed by a zone of increased energy as reflected in a grain size increase, rise in Si and decrease in Rb into zone C5. The basal chemical sub-zone displays an increase in Zr/Sr suggesting that a terrestrial input was initiated after the erosion, possibly as a result of water retreat seaward drawing a signal from the land. Above this zone six characteristic chemical sub-zone cycles (b–g) are identified, with a further sub-zone at the end of the sequence.

The six cycles are marked by increasing Si/Rb and Sr/Rb at the base (associated with increasing grain size and increasing shell content respectively) to a peak in the middle of the sub-zone, which then decreases (sediment fining-upwards as indicated by the reducing Si/Rb ratio) to the top of the sub-zone. Boundaries between sub-zones are identified by a minima in Si/Rb reflecting flow velocity stagnation. Sub-zones b, d and f all have higher Sr/Rb peaks and lower Zr/Sr peaks than sub-zones c, e and g. Sub-zone c, e and g also display higher Zr/Sr peaks. The relationship of all the ratios would suggest that the sediment in the former sub-zones have a dominant marine source and the latter a more terrestrial source. The minima between zones represents times of lowest energy or stagnation in energy between the events. The last sub-zone (h) also shows rising values in Zr/Sr, which, together with decreasing Si/Rb and Sr/Rb values, reduce to levels that were recorded in zone C6 prior to the sudden change within unit C5. Unit C4 contains high Rb values, low Sr and increasing Si values reflecting the transitional from fine to coarse material with little shell input. The sequence terminates by a unit that shows low Rb, the lowest Sr and the highest Si abundances seen in the core typical of recent marine sands.

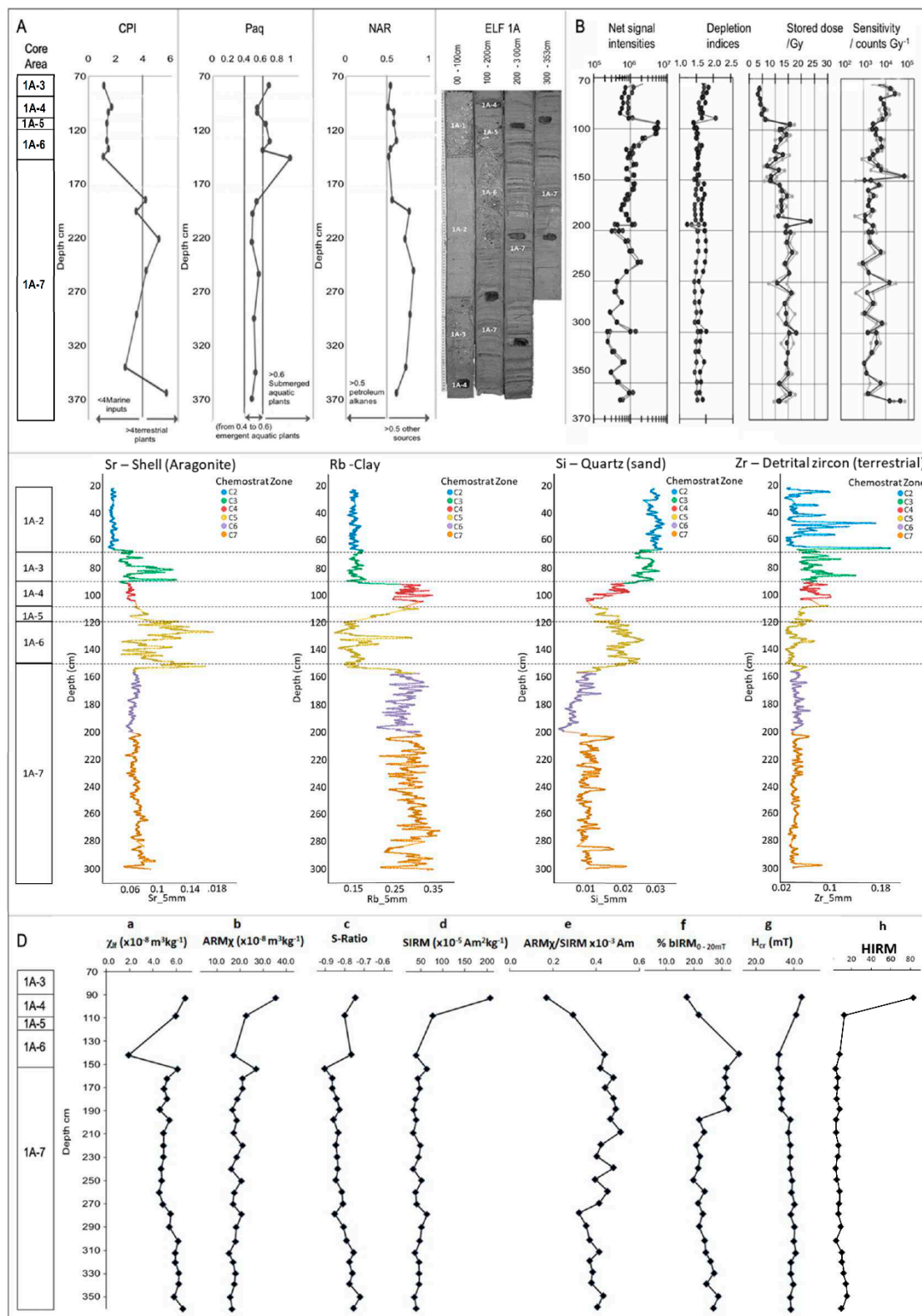


Figure 3. Geochemical analysis of vibrocore ELF001A. **A:** Organic chemistry profile. Carbon Preference Index (CPI) is an indicator of marine or terrestrial environments. N-alkane proxy ratio (Paq) distinguishes emergent and submerged aquatic plants. Natural alkanes ratio (NAR) distinguishes n-alkanes from natural oil sources from other sources such as higher plants. **B:** Optical stimulation luminescence (OSL). **C:** Chemostratigraphy based on chemical proxies for shell (Sr), Clay (Rb), Quartz grain size (Quartz/Clay; Si/Rb) and terrestrial material (Detrital zircons; Zr) **D:** Palaeomagnetism profile.

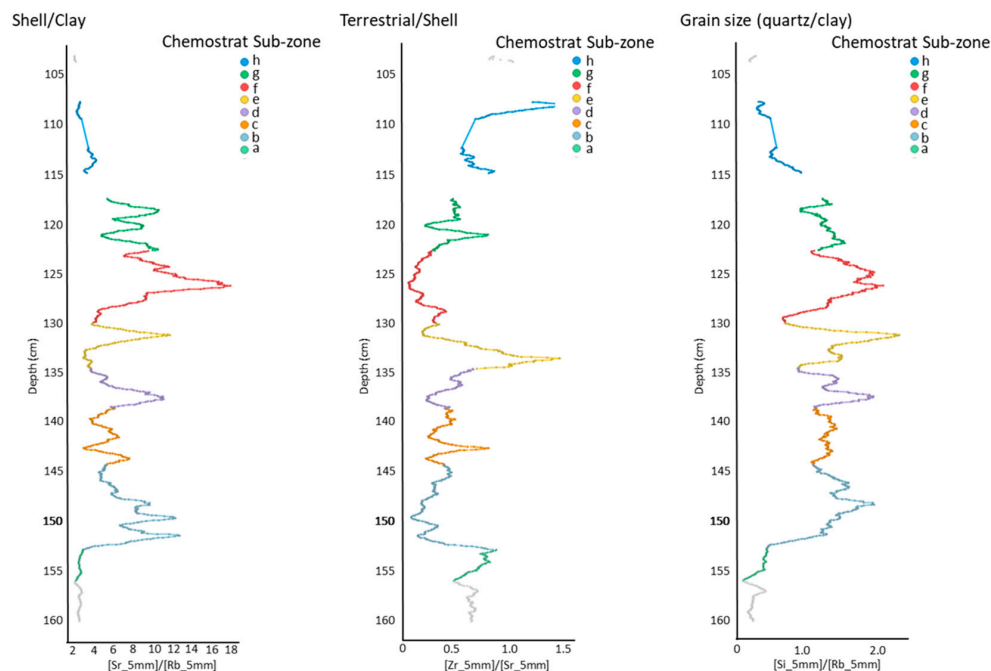


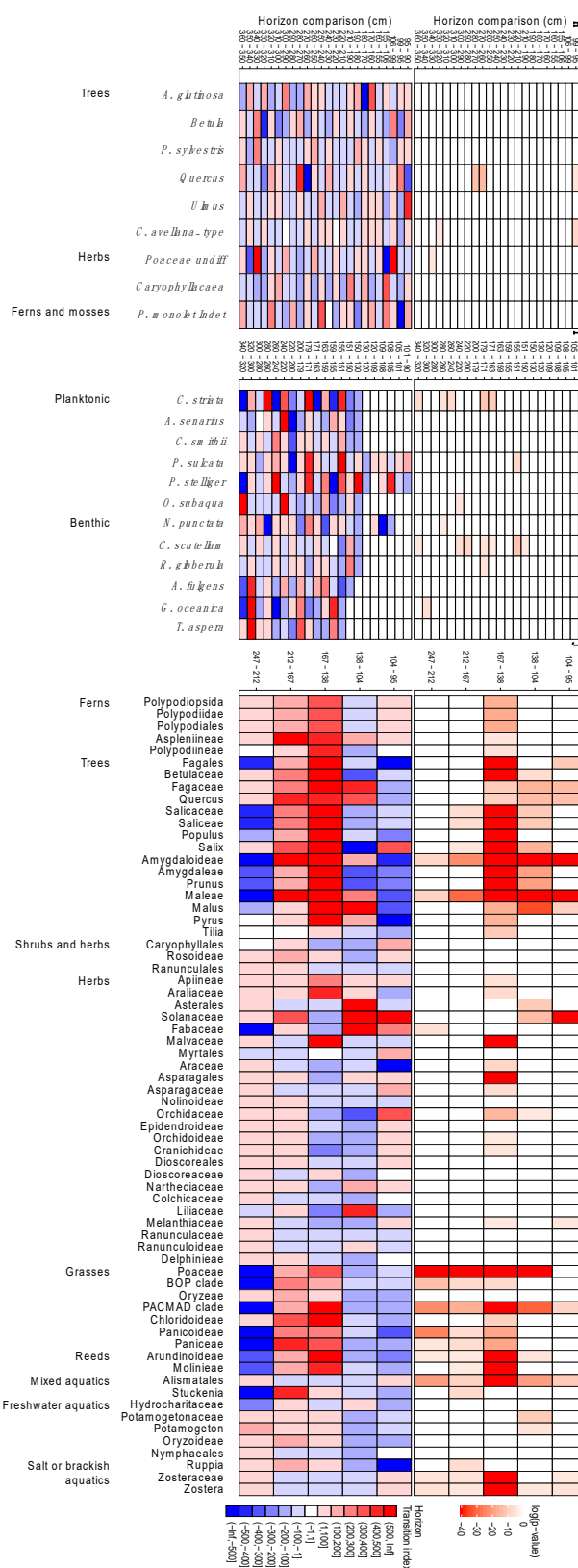
Figure 4. Proxy environmental data for key section (C3) of core ELF001A. Internal sub zones of geochemistry unit C3 showing eight sub units that form the chemical architecture of the tsunami deposit based on chemical proxies for shell (Sr), Clay (Rb), grain size (Quartz/Clay; Si/Rb) and terrestrial material (Detrital zircons; Zr).

The iron-bearing minerals in the sediments can relate to several factors in the depositional environment including the source, transport and deposition mechanisms of the sediment. Palaeomagnetic data taken from sub-samples at 0.1 m intervals show signatures associated with low or no change in the detrital input from the base of the core to approximately 1.50 m (Figure 3D). From approximately 1.10 m to 1.50 m the core is characterized by lower χ_{lf} values than the preceding unit, together with a reduction in fine-grained magnetite (ARM_{χ}). This suggests that the material is from a different origin to the local sediment supply as it contains a lower abundance of single domain particles. The S-ratio throughout this interval shows a higher concentration of haematite and goethite. However, this is not mirrored by the Hard IRM proxy or the coercivity of remanence, suggesting that the magnetic behaviour is the result of multi-domain magnetite co-existing with fine grained greigite. Above 1.10 m, SIRM and magnetic susceptibility suggest a much greater abundance of magnetic minerals.

4.4. Palaeoenvironmental Characterization of ELF001A

We further confirmed the nature and source of this stratum using multiple palaeoenvironmental proxies (Figure 5). Proxies included foraminifera, ostracods (SI Text S4.1), pollen (SI Text S4.2), diatoms (SI Text S4.3), molluscs (SI Text S4.4) and sedimentary ancient DNA (sedaDNA, SI Text S4.5). Relatively low levels of cytosine deamination and fragmentation patterns consistent with ancient DNA of this age and environment [23] were observed firstly by mapping sedaDNA to *Quercus*, *Corylus* and *Betula* genomes applying conventional mismatching approaches [24] (Figures S17 and S18), and secondly applying a novel metagenomic assessment methodology in which all sedaDNA is assessed for deamination damage, which may be more suitable for this data type (Figure S19). We then further tested sedaDNA for stratigraphic integrity to assess possible biomolecule vertical movement in the core column (Figure S20). Figure 5 shows that the sedaDNA demonstrates highly significant differentiation between strata indicating a lack of movement post deposition. Together, these tests indicate that authentic sedaDNA was retrieved and most likely represent the original depositional environment. Interestingly, the same stratigraphic tests applied to pollen generally show a lack of differentiation between strata, indicating both a consistent influx of pollen from the surrounding area

from oak, hazel woodland and that the sedaDNA derived from sources other than pollen, as has been previously suggested in other sedimentary contexts [25]. This suggests a taphonomy in which the sedaDNA represents a local signal relative to a more regional palynological signal.

Figure 5. *Cont.*

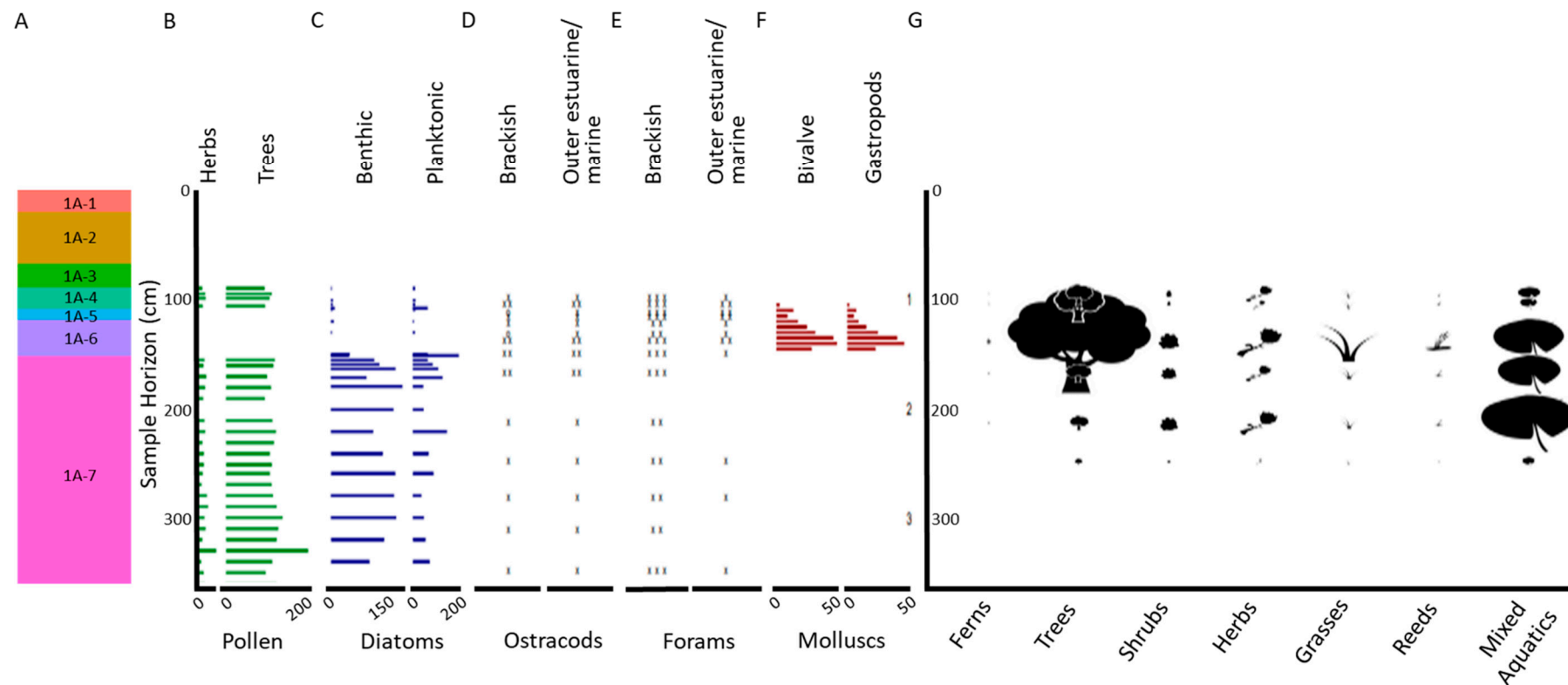


Figure 5. Assessment of taxon change between sample horizons of taxa with abundances >50, see Supplementary Information and SI Text S4.5 for methods. Top Panel—Probability of observed taxa counts between pairs of horizons being drawn from the same distribution. Middle Panel—Index of change between horizons based on changes in maximum likelihood estimators of the probability taxon being selected from each horizon. Blue indicates a decrease in probability moving up the core, red an increase. Bottom Panel—Palaeoenvironmental reconstruction where all measurements were taken from lithological units 1A-4 and below. A. Lithological units based on sediment types described in Supplementary Information, Figure S1 and Table S1. Panels B-G palaeoenvironmental proxy abundances, for detailed taxonomic break downs, see Supplementary Information, Table S12, Figures S16–S18 and S19B. Pollen counts. C. Diatom counts. D. Ostracod abundance E. Foraminifera abundance. Foraminifera and ostracods are recorded: o—one specimen; x—several specimens; xx—common; xxx—abundant. F. Mollusc counts. G. Plant sedaDNA vegetation type with icon size relative to biogenic mass.

The environment prior to this dramatic event, and recorded in the underlying stratum Unit 1A-7, was an estuarine mudflat typified by predominantly benthic epiphytic and epipellic diatom communities and brackish foraminifera and ostracods, with a sedaDNA floral profile of *Zostera* and *Potamogeton* as well as members of the Hydrocharitaceae and Araceae present. This was surrounded by an area with a strong meadow influence that is also apparent in the sedaDNA profile including buttercups, orchids, mallows and asterids. Further, an open woodland is suggested close by, Figure S20.

By contrast the underlying unit 1A-6 is characterized by an abrupt change in both microfossil and sedaDNA evidence. There is an absence of diatoms and pollen; an increase in outer estuarine or marine taxa of ostracods and foraminifera; the appearance of fractured molluscan shells from different and incompatible habitats including sublittoral, intertidal and brackish species; and the sudden and significant influx of all woody taxa in the sedaDNA profile (Figures S16 and S20 and Table S12). A novel measure of relative biomass, biogenomic mass, based on sedaDNA and genome size (Figure S20), suggests a higher biomass of trees than either *Zostera* or *Potamogeton* in this stratum, although these latter taxa dominate in other strata, Figure 5 (Figure S20). Together, these proxies indicate a violent event that brought with it the terrestrially derived debris of surrounding woodland.

After the event in units 1A-4 to 1A-1 the foraminifera and ostracod signal indicate a return to estuarine mudflats with a greater abundance of marine taxa such as *Ammonia batavus* indicating a more established marine signal than prior to the event, Table S12. The sedaDNA signal also indicates estuarine taxa such as *Zostera*, and a meadow influence, although the biogenomic mass appears greatly reduced suggesting more distant proximity of the flora. A faunal signal considerably weaker than the floral was present throughout the core, but shows a significant elevation in count towards the top units ($p = 1.0014 \times 10^{-6}$), indicating the presence of rodents and larger animals such as bear, boar and cloven hoofed ruminants, as well as higher orders of fish (Acanthomorpha, Eupercaria, Osteoglossocephalai), Figure S21.

4.5. Dating of Deposit

The depositional ages of the sequence in ELF001A was investigated using OSL (Figure 3B, SI Text 3.1) and directed AMS radiocarbon dating (SI Text 3.2). Luminescence stratigraphies generated for the core, with proxies of net OSL signal intensities and depletion indices (Figure 3B, columns 1 and 2) and OSL stored dose and sensitivity (Figure 3B, columns 3 and 4), contextualize depositional ages determined by quartz SAR OSL for units 1a-4 to 1a-7. Units 1A-6 and 1A-5 are dated by quartz SAR OSL to 8.04 ± 0.43 ka and 8.22 ± 0.43 ka, respectively, with a combined age of 8.14 ± 0.29 ka. The base of unit 1a-4 at 105 cm depth in core is dated to 7.16 ± 0.50 ka, and at 1.00m depth to 6.03 ± 0.22 ka.

Lithological units 1a-1 to 1a-7 are characterized by distinct luminescence behaviour described here from oldest to youngest. Unit 1a-7 is sub-divided into two further units, from 1.51 m to c. 2.00 m and deeper than 2.00 m. From 1.51 m to 2.00 m, the proxies show stratigraphic trends with depth indicating a more gradual accumulation than from c. 2.00 m to the base of the core where the proxies fluctuate around central tendencies marked by more rapid accumulation. Units 1a-5 and 1a-6 show a cyclicity with ‘couplets’ characterized by paired zones with low OSL intensities/high depletion indices and higher OSL intensities/low depletion indices. Within this unit inclusions of shell fragments were dated to 9.26–8.93 ka cal BP (at 95.4%; 8.34 ± 0.3 ka BP, Beta-505683) by radiocarbon AMS dating.

Unit 1a-4, shows a step-change in OSL intensities and stored doses across the 1a-4/1a-3 boundary demonstrating a change in depositional dynamics, and further that the quartz here was likely sourced from a different provenance. Units 1a-2 to 1a-3 show a normal signal-depth progression in these proxies resulting from gradual accumulation with no temporal breaks. Finally, Unit 1a-1 is characterized by fluctuating OSL intensities and variable OSL stored doses with no stratigraphic coherence showing these sands are derived from a highly mobile sequence.

5. Discussion

5.1. Interpretation of the Deposit within Core ELF001A

The combined data presented here lead us to suggest that this sequence is either the result of a sustained storm period or is consistent with the impact from a large tsunami event. A number of points may be raised here through comparison of features illustrated and interpreted in Figure 6 (also summarized in Table S3) with reference to the summary of criteria for recognition of tsunami derived deposits compared to those of storm surges presented in Table 1. Key characteristics include evidence for sediment grading, as indicated through the geochemical signatures, the source of material, in particular the multiple, repeated cycles of marine derived (shell dominated) fraction compared to the land derived fraction, and changes in flora and fauna as indicated by the sedaDNA within key sub-parts of the sequence.

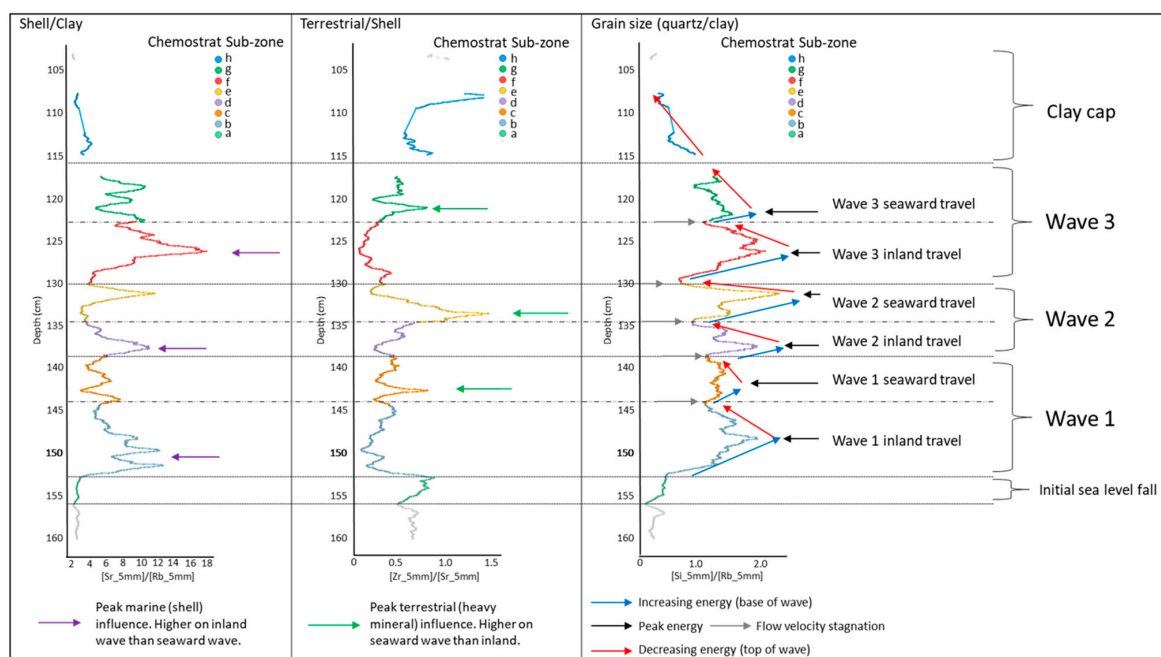


Figure 6. Interpretation of proxy environmental data for key section (C3) of core ELF001A. The initial sea level fall is marked by increased terrestrial material (green arrows). Waves are characterised by an increase of energy reflected by increased grainsize at the base (blue arrow), which peaks approximately in the centre of the sub unit (black arrow), before decreasing to a flow velocity (red arrow) to stagnation at the top of the sub unit (grey arrow). Inflow (towards land) water movement is characterised by the larger shell material peak (purple arrow) whereas retreat (seaward) movement is marked by a larger terrestrial signature. The end of the tsunami zone is marked by a clay cap where wave energy (velocity of flow) returns to minimum values.

The geochemical signatures of the key sequence (Figure 6) are interpreted to show three sets of marine dominated, landward travelling waves and terrestrial dominated, seaward travelling backwash similar to those described by Riou et al. [15]. For example, the ratio of Zr/Sr shown in our study can be compared to Ti/Ca ratio of Riou et al. [15] where Zr is overwhelmingly sourced within zircon, a heavy mineral that is terrestrially sourced as Ti is dominantly found in the heavy mineral Rutile. The marine component is expressed in our study by Sr as compared to Ca. The chemistry of the start of the sequence is consistent with draw-down from the land followed by six dominant cycles of fining-upwards deposition that are interpreted as a result of three main wave events.

Grain size for the whole of this 45 cm sequence is much greater than in the preceding zone. The sub-zone cycles that have been identified can be grouped into pairs, with the first in each showing

increased shell content (high Sr/Rb) and the second a higher terrestrial signature (high Zr/Sr) than the first. This pattern is consistent with that of a tsunami event where the wave impinges on the land depositing marine-dominated detritus, and then retreats leaving an enhanced terrestrial signature and does so in multiple wave events. For example, Bodevik et al. [4] identified similar multiple deposition events attributed to the Storegga tsunami within near-sea level basins on the Norwegian coast and Wagner et al. [26] interpreted four distinct wave sequences within deposits from a basin in East Greenland. This contrasts with the resulting deposits for a storm sequence that typically only deposit a single sedimentary sequence. This is also demonstrated in the sedaDNA which has identified woody taxa in this interval. In modern tsunami events it is often noted that the second wave is larger than the first, and the data presented here is consistent with such an observation. The highest terrestrial signal (Zr/Sr) is on the returning backwash (chemostratigraphic sub-zone e) following the second in-pulse (sub-zone d). This is mirrored in the OSL data; the intensity counts, at this point, are at a maximum for the entire core.

Palaeomagnetic data also indicate that the whole of this unit contains material that is not locally sourced; suggesting there has been a dramatic provenance change over the whole of this interval. The final phase of the sequence is marked by a return to conditions similar to that existing before the event and indicated through a reduction in grain size back to clay-silt. The sedaDNA data lead us to conclude the effects of the tsunami altered the immediate landscape. This may have included opening up the vegetation around channel margins allowing easier access to the streams to larger animals or a more major realignment of drainage networks. However, given the return of the terrestrial signal in subsequent strata we conclude that the final marine inundation occurred at a later time in this area. The return to salt marsh species after the event would further imply that there was not a general sea level increase through this event, as would have occurred if the deposit were a result of transgression for example from the global sea level rise associated with outburst of Lake Agassiz.

5.2. Geomorphological Influence on the Tsunami Propagation

The occurrence of a tsunami deposit at ELF001A, 42 km from its contemporary coastline (Figure 7) is unexpected given previous models have estimated a magnitude of wave that would reach 21 km inland in this area [6] before becoming impeded by a glacial moraine belt [20]. Our reconstruction at approximately 8.2 ka cal BP combined with the modelling of Hill et al. [6] suggests that the geomorphology of the landscape could have been instrumental in funnelling the wave inland and along the glacial tunnel valleys that breach the moraine. The Outer Dowsing Deep is one of these valleys (Figure 7) and the passage here is a steep sided U-shaped valley that becomes progressively deeper southwards, towards the central basin. This basin, being below the 8.2 ka cal BP sea level, supports the palaeoenvironmental proxy evidence for an estuarine system. Such a configuration is expected to lead to an intensification of the wave and consequently a significantly enhanced impact [27]. However, as Bondevik et al. [28] have noted, tsunami deposits in different situations ranging from subtidal through intertidal to onshore, are highly influenced by the morphology of the coast which can play an important role in determination of the nature of deposits at any one place in the landscape. For this reason, deposits may be evident at one location but absent in a nearby location and this is the case with some of the cores within this wider study.

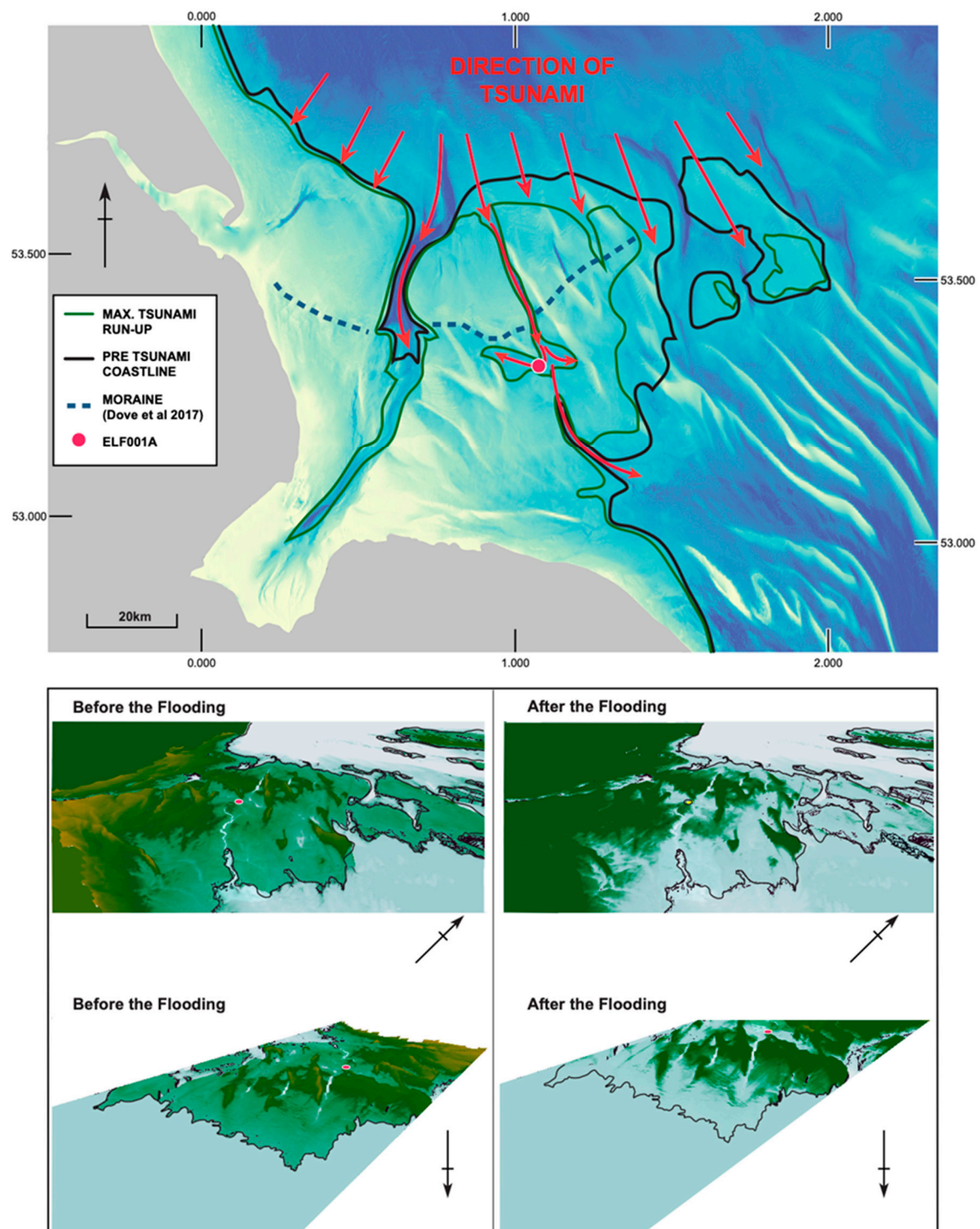


Figure 7. Geomorphological reconstruction of the palaeolandscape off the east coast of England c. 8.2 ka cal BP. Above: Coastline reconstruction at 8.2 ka cal BP and inferred direction of tsunami advance following the modelling of Hill et al. [6]. Below: 3D rendering of the area from northern and southern perspectives before and after inundation (arrow represents north direction).

5.3. Correlation of the Tsunami Event, the Storegga Slide and Final Inundation of Doggerland

The interpretation of the data from core ELF001A as a tsunami event is compelling. However, as Peters and Jaffe [15] indicate, the explanation of any sequences as the consequence of a tsunami should be informed by the geographic context for the deposits. In this case, the timing indicated

by both OSL and RC suggests a significant correlation with the Storegga Event and the subsequent tsunami dated at 8.15 ka cal BP [2].

The data also lead us to conclude that the current physical evidence for the Storegga tsunami in the study area is highly localized because of the channelling effect of the tunnel valley systems and barriers to wave propagation provided by the wooded glacial moraines. This restricted distribution was further reduced by later erosive processes. It may be the case that physical evidence for the Storegga tsunami in the southern North Sea has not been previously observed because it only resides in restricted locales, such as incised river systems, and where the geography and local conditions were favourable for preservation.

To explore this scenario further we tracked the probable height of the tsunami stratum from ELF001A across the landscape using Glacial Isostatic Adjustment models [19], seabed mapping and Geographic Information System analysis (SI Text 1.1 and SI Text 1.3). Seismic data was then used in order to predict where similar deposits would be expected to be preserved in other cores, Figure S1. The analysis indicated an absence of strata contemporaneous to the tsunami layer in many areas suggesting widespread erosion subsequent to the tsunami event. However, the seismic signal associated with the change in sediment density, and identified as the tsunami stratum in ELF001A, was used to trace other locations likely to contain signals originating from the same source (Figure S2). Whilst this further, detailed research is ongoing, two other tsunami candidate cores, ELF003 and ELF059A, were identified using this technique. These are situated within the central basin area and southern river channel, Figures S1 and S3. However, it should be noted that this signal was not replicated in other seismic surveys, and the signal, which correlates in this instance, cannot, as such, be regarded as diagnostic for the purposes of identifying the presence or absence of similar deposits elsewhere.

Further work, within the route of the Southern River system, as defined by palaeobathymetry, led to the identification for two further cores ELF031A and ELF039, as candidates to contain deposits in the outflowing channel to the south of the basin (SI Text 1.3). Although further study of these cores is ongoing, significant surges in woody taxa, similar to that seen in Unit 1A-6 at the predicted tsunami height, were detected in ELF003 and ELF0039 based on sedaDNA. The position in ELF0059A corresponding to the tsunami event occurred at the base of the core, and was also associated with a significantly higher abundance of woody taxa than overlying strata. ELF0031A yielded too little sedaDNA for interpretation, Figure S23. Radiocarbon dates from ELF003 confirmed the corresponding tsunami height to be contemporaneous with Unit 1A-6, supporting the notion that these cores carry a much-diminished signal of the tsunami event. Further research is needed to confirm such an interpretation.

5.4. Correlation of the Tsunami Event, the Storegga Slide and Final Inundation of Doggerland

Whilst the interpretation of the data from core ELF001A as a tsunami event is attractive, Peters and Jaffe [16] argue that the explanation of any sequences as the consequence of a tsunami should be informed by the geographic context for the deposits. In this case, the timing indicated by both OSL and RC suggests a significant correlation with the Storegga Event and the subsequent tsunami dated at 8.15 ka cal BP [2]. The identification of multiple wave events as the characteristic sequence of the deposits here are similar to those reported elsewhere as a result of the Storegga event [28]. Furthermore, the thickness of the sequence recorded is less than the 70 cm thick deposits reported in East Greenland by Wagner et al. [26]. It should be noted however that while both the East Greenland location and that described here are both approximately 1200 km from the Storegga event, the East Greenland site is in direct line along the Storegga slip plane. The data also lead us to conclude that the current physical evidence for the Storegga tsunami in the study area is highly localized because of the channelling effect of the tunnel valley systems and barriers to wave propagation provided by the wooded glacial moraines. This restricted distribution was further reduced by later erosive processes. It may be the case that physical evidence for the Storegga tsunami in the southern North Sea has not been previously observed because it only resides in restricted locales, such as incised river systems, and where the geography and local conditions were favourable for preservation.

6. Conclusions

Our evidence shows that the Storegga tsunami impacted coastlines in the area of the southern North Sea covered by this study. In these coastal areas, where Mesolithic human populations may have resided for most of the year, settlement would have been badly affected. The multi-proxy evidence suggests the landscape recovered temporarily and hence confirms that the final submergence of the remnant parts of Doggerland occurred after the Storegga tsunami. At the same time, the remaining local terrestrial landscape is suggested to have been more open or that realignment of the drainage networks was responsible for bringing in sedaDNA from more open contexts. Occupation could therefore have continued after the tsunami retreated, but within a much-modified coastal landscape before early-mid Holocene eustatic sea-level rise was responsible for finally submerging the remnant Doggerland lowlands and its associated Mesolithic communities.

The multi-proxy methodological approach applied to the analysis of cores within this project has provided one of the most complete data sets for investigation of tsunami morphology to date. The approach is not typical in either terrestrial or marine investigations but is to be recommended if the maximum information about past changing landscapes is to be gained. Further, the approach holds great promise for wide area reconstructions of palaeogeography, environments and human occupancy where a greater understanding of the impact of large natural events is needed.

Supplementary Materials: The following are available online at www.mdpi.com/xxx/s1, Geomorphological analysis including seismic, coring and palaeobathymetry are presented in SI supplementary SI Text 1. Geochemistry analysis including palaeomagnetism, elemental core scans and organic chemistry profiling are presented in SI supplementary SI Text 2. Dating of sediments using OSL and organic materials using radiocarbon is presented in SI supplementary SI Text 3. Palaeoenvironmental analysis including foraminifera, ostracods, pollen, diatoms, molluscs and sedaDNA are presented in SI supplementary SI Text 4.

Author Contributions: Study conceptualized and design: V.G., S.F., M.B., R.B. and R.G.A.; Geomorphology and seismic: S.F., R.B., M.M.; Lithography and geology: M.B., S.F., V.G., R.B.; Geochemistry: A.F., R.T., C.B., B.S., M.B.S., S.D., S.H.; OSL dating: T.K.; AMS radio carbon dating: D.H.; sedaDNA: R.L.W., R.E., R.G.A., R.C., L.K.; Palaeoenvironmental proxies (pollen, diatom ostracods, foraminifera, molluscs): B.G., T.H., J.W. (John Whittaker), K.K., M.B.; Archaeology: J.W. (James Walker), S.F. and V.G.; Manuscript drafting: R.G.A., V.G., R.B., M.M. and S.F. with some input from L.K.; Information on Mollusca: M.L. All authors have read and agreed to the published version of the manuscript.

Funding: This project has received funding from the European Research Council (ERC) under the European Union's Horizon 2020 research and innovation programme (ERC funded project No. 670,518 'Europe's Lost Frontiers Project', https://europea.eu/european-union/index_en, <https://lostfrontiers.teamapp.com/>). The project gratefully acknowledges the support of the Estonian Research Council (<https://www.etag.ee/en/estonian-research-council/>, Grant number: PUTJD829). PGS (<https://www.pgs.com/>) is acknowledged through provision of data used in this paper under license CA-BRAD-001-2017.

Acknowledgments: The authors acknowledge the careful review of the manuscript by anonymous reviewers and are also grateful for comments on earlier drafts by Tim Raub.

Conflicts of Interest: The authors declare no conflicts of interest

References

1. Coles, B. Doggerland: A speculative survey. *Proc. Prehist. Soc.* **1998**, *64*, 45–81. [[CrossRef](#)]
2. Weninger, B.; Schulting, R.; Bradtmöller, M.; Clare, L.; Collard, M.; Edinborough, K.; Hilpert, J.; Jöris, O.; Niekus, M.; Rohling, E.J.; et al. The catastrophic final flooding of Doggerland by the Storegga Slide tsunami. *Doc. Praehist.* **2008**, *35*, 1–24. [[CrossRef](#)]
3. Waddington, C.; Wicks, K. Resilience or wipe out? Evaluating the convergent impacts of the 8.2 ka event and Storegga tsunami on the Mesolithic of northeast Britain. *J. Archaeol. Sci. Rep.* **2017**, *14*, 692–714. [[CrossRef](#)]
4. Bondevik, S.; Svendsen, J.I.; Johnsen, G.; Mangerud, J.; Kaland, P.E. The Storegga tsunami along the Norwegian coast, its age and runup. *Boreas* **1997**, *26*, 29–53. [[CrossRef](#)]
5. Fruergaard, M.; Piasecki, S.; Johannessen, P.; Noe-Nygaard, N.; Andersen, T.J.; Pejrup, M.; Nielsen, L. Tsunami propagation over a wide, shallow continental shelf caused by the Storegga slide, southeastern North Sea, Denmark. *Geology* **2015**, *43*, 1047–1050. [[CrossRef](#)]

6. Hill, J.; Avdis, A.; Mouradian, S.; Collins, G.S.; Piggott, M. Was Doggerland catastrophically flooded by the Mesolithic Storegga tsunami? *arXiv* **2017**, arXiv:1707.05593.
7. Bondevik, S.; Løvholt, F.; Harbitz, C.; Mangerud, J.; Dawson, A.; Svendsen, J.I. The Storegga Slide tsunami—Comparing field observations with numerical simulations. *Mar. Pet. Geol.* **2005**, *22*, 195–209. [[CrossRef](#)]
8. Walker, J.; Gaffney, V.; Fitch, S.; Muru, M.; Fraser, A.; Bates, M.; Bates, R. A Great Wave: The Storegga Tsunami and the end of Doggerland? *Antiquity* **2020**, in press.
9. Dawson, A.G.; Stewart, I. Tsunami deposits in the geological record. *Sediment. Geol.* **2007**, *200*, 166–183. [[CrossRef](#)]
10. Fujiwara, O.; Kamataki, T. Identification of tsunami deposits considering the tsunami waveform: An example of subaqueous tsunami deposits in Holocene shallow bay on southern Boso Peninsula, Central Japan. *Sediment. Geol.* **2007**, *200*, 295–313. [[CrossRef](#)]
11. Nanayama, F.; Shigeno, K.; Satake, K.; Shimokawa, K.; Koitabashi, S.; Miyasaka, S.; Ishii, M. Sedimentary differences between the 1993 Hokkaido-nansei-oki tsunami and the 1959 Miyakojima typhoon at Taisea, southwestern Hokkaido, northern Japan. *Sediment. Geol.* **2000**, *135*, 255–264. [[CrossRef](#)]
12. Kortekaas, S.; Dawson, A.G. Distinguishing tsunami and storm surge: An example from Martinhal, SW Portugal. *Sediment. Geol.* **2007**, *200*, 208–221. [[CrossRef](#)]
13. Goff, J.; McFadgen, B.G.; Chagué-Goff, C. Sedimentary differences between the 2002 Easter storm and the 15th century Okoropunga tsunami, southeastern North Island, New Zealand. *Mar. Geol.* **2002**, *204*, 235–250. [[CrossRef](#)]
14. Morton, R.A.; Gelfenbaum, G.; Jaffe, B.E. Physical criteria for distinguishing sandy tsunami and storm deposits using modern examples. *Sediment. Geol.* **2007**, *200*, 184–207. [[CrossRef](#)]
15. Riou, B.; Chaumillon, E.; Chagué, C.; Sabatier, P.; Schneider, J.; Walsh, J.; Zawadzki, A.; Fierro, D. Backwash sediment record of the 2009 South Pacific Tsunami and 1960 Great Chilean Earthquake Tsunami. *Nat. Sci. Rep.* **2020**, *10*, 1–13. [[CrossRef](#)]
16. Peters, R.; Jaffe, B. *Identification of Tsunami Deposits in the Geologic Record; Developing Criteria Using Recent Tsunami Deposits*; U.S. Geological Survey Open-File Report 2010-1239; Pacific Coastal and Marine Science Center: Santa Cruz, CA, USA, 2010; p. 39.
17. Dawson, A.G.; Shi, S. Tsunami deposits. *Pure Appl. Geophys.* **2000**, *157*, 875–897. [[CrossRef](#)]
18. European Marine Observation and Data Network (EMODnet) Digital Bathymetry (DTM2018). Available online: <https://sextant.ifremer.fr/record/18ff0d48-b203-4a65-94a9-5fd8b0ec35f6/> (accessed on 20 August 2018).
19. Bradley, S.L.; Milne, G.A.; Shennan, I.; Edwards, R.J. An improved glacial isostatic adjustment model for the British Isles. *J. Quat. Sci.* **2011**, *26*, 541–552. [[CrossRef](#)]
20. Dove, D.; Evans, D.; Lee, J.; Roberts, D.; Tappin, D.; Mellett, C.; Long, D.; Callard, L. Phased occupation and retreat of the last British-Irish Ice Sheet in the southern North Sea; geomorphic and seismostratigraphic evidence of a dynamic ice lobe. *Quat. Sci. Rev.* **2017**, *163*, 114–134. [[CrossRef](#)]
21. Fortin, D.; Francus, P.; Gebhardt, A.C.; Hahn, A.; Kliem, P.; Lisé-Pronovost, A.; Roychowdhury, R.; Labrieg, J.; St-Ongebe, G.; The PASADO Science Team. Destructive and non-destructive density determination: Method comparison and evaluation from the Laguna Potrok Aike sedimentary record. *Quat. Sci. Rev.* **2012**, *71*, 147–153. [[CrossRef](#)]
22. Chagué-Goff, C.; Szczuciński, W.; Shinozaki, T. Applications of geochemistry in tsunami research: A review. *Earth-Sci. Rev.* **2017**, *165*, 203–244. [[CrossRef](#)]
23. Kistler, L.; Ware, R.; Smith, O.; Collins, M.; Allaby, R. A new model for ancient DNA decay based on paleogenomic meta-analysis. *Nucleic Acids Res.* **2017**, *45*, 6310–6320. [[CrossRef](#)] [[PubMed](#)]
24. Jónsson, H.; Ginolhac, A.; Schubert, M.; Johnson, P.L.F.; Orlando, L. mapDamage2.0: Fast approximate Bayesian estimates of ancient DNA damage parameters. *Bioinformatics* **2013**, *29*, 1682–1684. [[CrossRef](#)] [[PubMed](#)]
25. Willerslev, E.; Cappellini, E.; Boomsma, W.; Nielsen, R.; Hebsgaard, M.B.; Brand, T.B.; Hofreiter, M.; Bunce, M.; Poinar, H.N.; Dahl-Jensen, D.; et al. Ancient Biomolecules from Deep Ice Cores Reveal a Forested Southern Greenland. *Science* **2007**, *317*, 111–114. [[CrossRef](#)] [[PubMed](#)]
26. Wagner, B.; Bennike, O.; Klug, M.; Cremer, H. First indication of Storegga tsunami deposits from East Greenland. *J. Quat. Sci.* **2006**, *22*, 321–325. [[CrossRef](#)]

27. Didenkulova, I.; Pelinovsky, E. Runup of tsunami waves in U-shaped bays. *Pure Appl. Geophys.* **2010**, *168*, 1239–1249. [[CrossRef](#)]
28. Bondevik, S.; Svendsen, J.I.; Mangerud, J. Tsunami sedimentary facies deposited by the Storegga tsunami in shallow marine basins and coastal lakes, western Norway. *Sedimentology* **1997**, *44*, 1115–1131. [[CrossRef](#)]



© 2020 by the authors. Licensee MDPI, Basel, Switzerland. This article is an open access article distributed under the terms and conditions of the Creative Commons Attribution (CC BY) license (<http://creativecommons.org/licenses/by/4.0/>).